Dynamic behaviour of a rotating cracked beam

Ahmed Yashar, Maryam Ghandchi-Tehrani and Neil Ferguson

Institute of Sound and Vibration Research, University of Southampton, Southampton SO17 1BJ, UK

E-mail: amiy1g14@soton.ac.uk

Abstract. This paper presents a new approach to investigate and analyse the vibrational behaviour of cracked rotating cantilever beams, which can for example represent helicopter or wind turbine blades. The analytical Hamiltonian method is used in modelling the rotating beam and two numerical methods, the Rayleigh-Ritz and FEM, are used to study the natural frequencies and the mode shapes of the intact rotating beams. Subsequently, a crack is introduced into the FE model and simulations are performed to identify the modal characteristics for an open cracked rotating beam. The effect of various parameters such as non-dimensional rotating speed, hub ratio and slenderness ratio are investigated for both the intact and the cracked rotating beam, and in both directions of chordwise and flapwise motion. The veering phenomena in the natural frequencies as a function of the rotational speed and the buckling speed are considered with respect to the slenderness ratio. In addition, the mode shapes obtained for the flapwise vibration are compared using the modal assurance criterion (MAC). Finally, a new three dimensional design chart is produced, showing the effect of crack location and depth on the natural frequencies of the rotating beam. This chart will be subsequently important in identifying crack defects in rotating blades.

1. Introduction

Rotating beams play a substantial part in various technological applications such as gas turbine blades, helicopter propellers and wind turbines. Fractures are most common faults in these structures that might contribute to increased vibration, which can ultimately cause complete failure. Investigations are made regarding the vibrational behaviour of a cracked rotating blade, which include crack identification and detection methods so that subsequent damage could be prevented. Numerous studies have investigated the effect of the rotational speed on the natural vibration of cantilever beams. These studies concluded that the natural frequencies of flexural vibration tended to increase above those for the non-rotating beams because of the centrifugal force and resulting stiffening effects [1]. The free vibration analysis of rotating beams have been widely studied [1–11]. However, the analysis of rotating cracked beams are relatively scarce in the literature [12, 13]. The objective of this paper is to develop a method to model a cracked rotating cantilever beam. Initially, the uncracked rotating beam is modelled using a simple continuous beam (the equilibrium of forces) based on Hamiltonian principle to find the governing differential equations [6]. Then, a finite element method and Rayleigh Ritz method are used to obtain the numerical results for a rotating intact beam. Subsequently, a crack element is introduced using fracture mechanics as presented by Qiau [14] and Behera [15] to the finite element model to calculate the effect of the crack on the rotating system. Finally, a parametric study is carried out for a cracked rotating beam using parameters such as the rotational speed,

the crack location, the hub ratio and the slenderness ratio.

2. Theoretical modelling of a rotating cracked beam

2.1. Modelling of a rotating beam

The equation of motion for the lateral vibration of a uniform thin homogeneous beam subjected to an axial force can be written as;

$$\rho A\frac{\partial^2 w}{\partial t^2}+\frac{\partial^2}{\partial x^2}\left(EI\frac{\partial^2 w}{\partial x^2}\right)-\frac{\partial}{\partial x}\left(P\frac{\partial w}{\partial x}\right)=f(x,t) \tag{1}$$

where ρ, A, E, I, w, P and f represent the mass density, cross sectional area, modulus of elasticity, second moment of area, transverse displacement, longitudinal (axial) force and transverse lateral distributed force, respectively. For free vibration, uniform cross section and constant P with respect to time, (1) can be rewritten as,

$$\rho A\frac{\partial^2 w}{\partial t^2}+EI\frac{\partial^4 w}{\partial x^4}-\frac{\partial}{\partial x}\left(P\frac{\partial w}{\partial x}\right)=0 \tag{2}$$

where r is the radius of the hub and x is the distance along the beam measured from the hub.

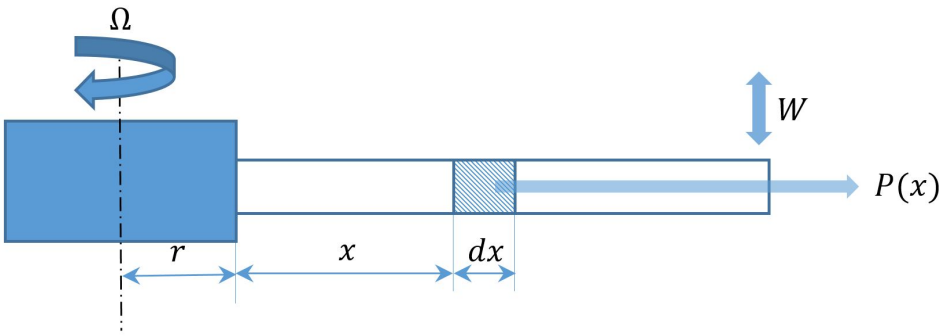

Figure 1. Lateral vibration of the beam subjected to an axial force. $P(x)$

For a rotating beam, the axial force P is due to and equal to the centrifugal force in Figure 1 and can be obtained as a function of position x along the beam from,

$$P(x)=\int_x^L \rho A\Omega^2(x+r)dx=\frac{1}{2}\rho A\Omega^2\{r(L-x)-\frac{1}{2}(L^2-x^2)\} \tag{3}$$

The equation of motion for the transverse vibration of the rotating beam then can be obtained by substituting (3) into (2);

$$\rho A\frac{\partial^2 w}{\partial t^2}+EI\frac{\partial^4 w}{\partial x^4}-\frac{1}{2}\rho A\Omega^2\frac{\partial}{\partial x}\left\{[r(L-x)-\frac{1}{2}(L^2-x^2)]\frac{\partial w}{\partial x}\right\}=0 \tag{4}$$

For the free vibration of the rotating beam, a harmonic solution with the frequency of ω and amplitude of W of the separable following form is assumed.

$$w(x,t)=W(x)\cos(\omega t) \tag{5}$$

Substituting the solution, Eq.(5), into Eq.(4) yields,

$$\rho AW\omega^2 + EI\frac{d^4W}{dx^4} - \frac{1}{2}\rho A\Omega^2\frac{d}{dx}\left\{[r(L-x) - \frac{1}{2}(L^2-x^2)]\frac{dW}{dx}\right\} = 0 \tag{6}$$

and the boundary conditions are assumed to be as follows for a cantilever ;

$$\begin{aligned} W(x) = \frac{dW(x)}{dx} = 0 \quad , \quad x = 0 \\ \frac{d^2W(x)}{dx^2} = \frac{d^3W(x)}{dx^3} = 0 \quad , \quad x = L \end{aligned} \tag{7}$$

The exact solution of Eq.(6) is difficult to obtain analytically due to the inclusion of the centrifugal force and the term $\frac{d}{dx}(x^2\frac{dw}{dx})$, which is equal to $2x\frac{dw}{dx} + x^2\frac{d^2w}{dx^2}$. Nevertheless, an approximate method using a numerical method such as the finite element method or Rayleigh-Ritz method can be used to solve this equation.

Figure 2 shows a rotating cantilever beam with a rigid hub rotating with angular velocity Ω about the vertical axis Z. The cantilever beam's length is along the X axis. The chordwise vibration occurs in the XY plane, parallel to the plane of rotation and perpendicular to the flapwise vibration which occur in the XZ plane. The coordinate system XYZ is fixed to the hub as shown in figure 2.

The displacement of point A to A' can be expressed in terms of the component displacements u, v and w where they correspond to the axial, chordwise and flapwise deformation, respectively. There is a geometrical relation between the length of the beam before and after the deformation as given in [16] by

$$x + s = \int_0^{x+u_x}\left[1 + \left(\frac{\partial u_y}{\partial \eta}\right)^2 + \left(\frac{\partial u_z}{\partial \eta}\right)^2\right]^{\frac{1}{2}} d\eta \tag{8}$$

where s represents the change in beam's length (stretch) and η is a dummy variable. The velocity of the point A in figure 3, can also be found from,

$$v_A = (\dot{u} - \Omega u_y)i + [\dot{v} + \Omega(r + x + u_x)]j + \dot{w}k \tag{9}$$

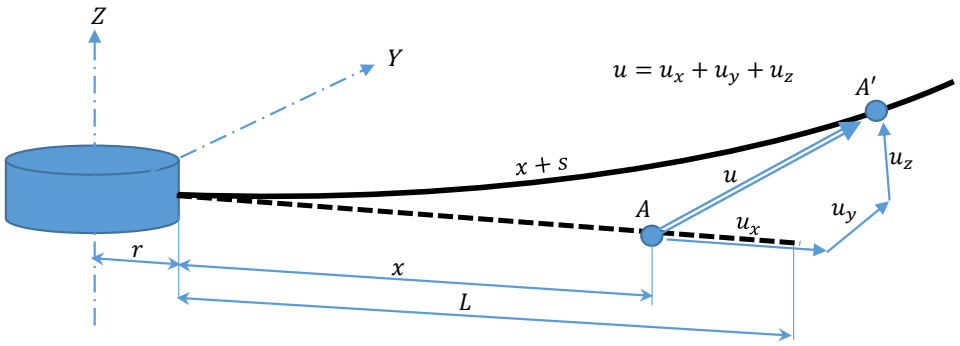

Figure 2. Configration of a rotating cantilever beam.

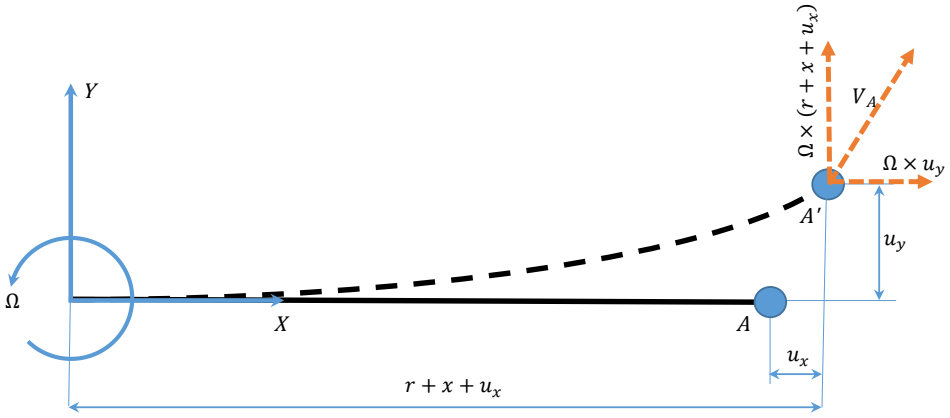

Figure 3. Top view of the system shown the relation between the angular and linear velocity.

Following the result by Kim et al [11], leads to a set of non-linear partial differential equations. After simplifying the differential equations and linearisation by neglecting higher order terms in the displacements, the following partial differential equations can be derived.

$$\rho A\left(\frac{\partial^2 s}{\partial t^2} - 2\Omega\frac{\partial v}{\partial t} - \Omega^2 s - \dot{\Omega} v\right) - EA\frac{\partial^2 s}{\partial x^2} = \rho A\Omega^2(a+x) + p_s \tag{10}$$

$$\rho A\left(\frac{\partial^2 v}{\partial t^2} - 2\Omega\frac{\partial s}{\partial t} - \Omega^2 v - \dot{\Omega} s\right) + EI_z\frac{\partial^4 v}{\partial x^4} - \rho A\Omega^2\frac{\partial}{\partial x}\left(r(L-x) + \frac{1}{2}(L^2 - x^2)]\frac{\partial v}{\partial x}\right) = p_v \tag{11}$$

$$\rho A\frac{\partial^2 w}{\partial t^2} + EI_y\frac{\partial^4 w}{\partial x^4} - \rho A\Omega^2\frac{\partial}{\partial x}\left([r(L-x) + \frac{1}{2}(L^2 - x^2)]\frac{\partial w}{\partial x}\right) = p_w \tag{12}$$

where p_s , p_v and p_w are the applied forces per unit length along the beam and in the y and z directions and I_y, I_z are the second moment of area about the y and z directions. It is interesting that Eq.(10) and Eq.(11) are coupled together, while Eq.(12) is independent of the other two. The boundary conditions from Eq.(7) are given by

$$\begin{aligned} s = v = w = \frac{\partial v}{\partial x} = \frac{\partial w}{\partial x} = 0 \quad , \quad x = 0, \\ \frac{\partial s}{\partial x} = \frac{\partial^2 v}{\partial x^2} = \frac{\partial^2 v}{\partial x^2} = \frac{\partial^3 v}{\partial x^3} = \frac{\partial^3 w}{\partial x^3} = 0 \quad , \quad x = L. \end{aligned} \tag{13}$$

A solution which satisfies the governing equation of motion together with the boundary conditions at every point over the domain is known as a strong form of solution. Conversely, a weak form of solution satisfies the conditions in an integral sense.

Following this step, the weak forms need to be obtained from the strong forms that are given by the partial differential equations and the corresponding boundary conditions. To derive the weak forms for the equation of motions for the Euler-Bernoulli beam, Eqs.(10)-(12) are multiplied by the weighting functions $\bar{s}$, $\bar{v}$ and $\bar{w}$ respectively, summed and integrated over the length L as follows.

For the chordwise

$$\rho A \int_0^L \left[\bar{s} \left(\frac{\partial^2 s}{\partial t^2} - 2\Omega \frac{\partial v}{\partial t} - \Omega^2 s - \dot{\Omega} v \right) + \bar{v} \left(\frac{\partial^2 v}{\partial t^2} - 2\Omega \frac{\partial s}{\partial t} - \Omega^2 v - \dot{\Omega} s \right) \right] dx$$
$$+ \int_0^L \left(EA \frac{\partial \bar{s}}{\partial x} \frac{\partial s}{\partial x} + EI \frac{\partial^2 \bar{v}}{\partial x^2} \frac{\partial^2 v}{\partial x^2} \right) dx$$
$$+ \rho A \Omega^2 \int_0^L \left[r(L-x) + \frac{1}{2}(L^2 - x^2) \right] \frac{\partial \bar{v}}{\partial x} \frac{\partial v}{\partial x}$$
$$= \int_0^L \{ \rho A \Omega^2 (r+x) \bar{s} + [p_v - \rho A \bar{\Omega} (r+x)] \bar{v} \} dx. \quad (14)$$

and for the flapwise

$$\rho A \int_0^L \frac{\partial^2 w}{\partial t^2} dx + EI_y \int_0^L \frac{\partial^2 \bar{w}}{\partial x^2} \frac{\partial^2 w}{\partial x^2} dx$$
$$+ \rho A \Omega^2 \int_0^L \left[r(L-x) + \frac{1}{2}(L^2 - x^2) \right] \frac{\partial \bar{w}}{\partial x} \frac{\partial w}{\partial x} dx$$
$$= \int_0^L \bar{w} p_w dx. \quad (15)$$

The displacements and weighting functions are now approximated by the shape functions as

$$\begin{aligned} \bar{s} &= (\bar{d}_e^{sv})^T N_s^T; s = N_s d_e^{sv} \\ \bar{v} &= (\bar{d}_e^{sv})^T N_v^T; v = N_v d_e^{sv} \\ \bar{w} &= (\bar{d}_e^{w})^T N_w^T; w = N_w d_e^{w} \end{aligned} \quad (16)$$

where d_e^{sv} and d_e^w are the element displacement vector for chordwise and flapwise, respectively. $\bar{d}_e^{sv}$and $\bar{d}_e^w$ are arbitrary vectors with the same dimensions of d_e^{sv} and d_e^w correspondingly. Finally N_s,N_v and N_w represent the trial shape functions.

Introducing these approximate solutions given by equations (16) in the weak equations given by Eq.(14) and Eq.(15), the equations can also be written in a matrix form, yielding the discretized equation for the chordwise and flapwise motion as,

$$\sum_{e=1}^{N} (d_e^{sv})^T \{ m_e^{sv} \ddot{d}_e^{sv} + 2\Omega g_e^{sv} \dot{d}_e^{sv} + [k_e^{sv} + \Omega^2 (s_e^{sv} - m_e^{sv}) + \dot{\Omega} g_e^{sv}] d_e^{sv} \} = \sum_{e=1}^{N} (d_e^{sv})^T f_e^{sv} \quad (17)$$

$$\sum_{e=1}^{N} (d_e^{w})^T [m_e^{w} \ddot{d}_e^{w} + (k_e^{w} + \Omega^2 s_e^{w}) d_e^{w}] = \sum_{e=1}^{N} (d_e^{w})^T f_e^{w} \quad (18)$$

where m_e^{sv}, g_e^{sv}, k_e^{sv} and s_e^{sv} are terms in the element mass, the element gyroscopic, the element stiffness and motion-induced stiffness matrices for the chordwise motion. Meanwhile, m_e^w, k_e^w and s_e^w are the corresponding terms for flapwise motion. f_e^{sv} and f_e^w are the element load vectors for the chordwise and flapwise motions.

The weak form solution and approach converts the continuous system into discrete elements, which can have a finite number of degrees of freedom and can be solved by a finite element

method or by given shape functions using the Rayleigh-Ritz method. However, the next step is to represent the system by matrices and convert continuous equations of motion by the weak form into the equation of motion based on the mass and stiffness matrices. This can be obtained by introducing s_e, v_e and w_e into the above equations. These three terms represent the elements' displacements in the stretch, chordwise and flapwise directions, respectively, and they refer to the local deformation of the discrete element.

2.2. Modelling of a crack

According to fracture mechanics theory, an open crack in a structure can be considered as a source of additional local flexibility because of the increase in the strain energy in the area surrounding the crack tip. The idea of substituting massless springs instead of a crack is to create the relation between the strain energy and the applied loads as shown in figure 4. The flexibility coefficients are stated in terms of stress intensity factors (SIF).

Applying Castigliones theorem [17, 18], figure 5 shows the generalized loading conditions for a beam of rectangular cross section with an open edge surface crack. The beam is loaded statically with an axial force, P_1, shear forces, P_2 and P_3, bending moments, P_4 and P_5, and torsional torque, P_6. However, determining the additional flexibility can be achieved using Hooke's law, which relates the stiffness to the acting force and the deflection displacement. The flexibility can also be calculated from Eq.(19).

$$c_{ij} = \frac{\partial \delta_i}{\partial P_j}, (i, j = 1, 2, 3). \tag{19}$$

where c_{ij}, δ, Π_c and P_i represent the additional flexibility, the displacement, the additional strain energy and the applied loads respectively, and can be obtained from,

$$\delta = \frac{\partial \Pi_c}{\partial P_i} \tag{20}$$

$$\Pi_c = \int_{A_c} G dA \tag{21}$$

where A_c is the effective crack area and G is the strain energy release rate function expressed as [19].

$$G = \frac{1}{E'} \left[\left(\sum_{i=1}^{n} K_{Ii} \right)^2 + \left(\sum_{i=1}^{n} K_{IIi} \right)^2 + \left(\sum_{i=1}^{n} K_{IIIi} \right)^2 \right]. \tag{22}$$

For plane stress problem [18] $E' = E$ and for the plane strain problem $E' = E/(1 - \mu^2)$, Ks are the stress intensity factors (SIF) due to forces. I, II, III represent the modes of the crack namely opening, sliding and tearing respectively, and $i = 1, 2, 3, ..., n$ related to the applied loads on the beam $P_1, P_2, P_3, ..., P_n$. In this study, the in-plane vibration beam model is developed. The applied forces are shown in figure 6. Rearranging Eq.(22) to match in-plane strain energy release rate function [20], yields

$$G = \frac{1}{E'} \left[(K_{I1} + K_{I2} + K_{I3})^2 + (K_{II2})^2 \right]. \tag{23}$$

According to Ozturk et al [21], the SIF for each force and mode becomes,

$$K_{I1} = \frac{P_1}{bh}\sqrt{\pi\xi}F_1 \tag{24}$$

$$K_{I2} = \frac{3P_2L_c}{bh^2}\sqrt{\pi\xi}F_I \tag{25}$$

$$K_{I3} = \frac{6P_3}{bh^2}\sqrt{\pi\xi}F_I \tag{26}$$

$$K_{II2} = \frac{P_2}{bh}\sqrt{\pi\xi}F_{II} \tag{27}$$

where ξ is the crack depth, F_i is the correction factors of the SIF. Notice that a is the final crack depth, whereas ξ is the depth within process of ongoing from zero crack depth to distance a.

$$F_1 = \sqrt{\frac{2}{\pi\xi}\tan\frac{\pi\xi}{2}}\frac{0.752 + 2.02\xi + 0.37\left[1 - \sin\left(\frac{\pi\xi}{2}\right)\right]^3}{\sqrt{\cos\left(\frac{\pi\xi}{2}\right)}} \tag{28}$$

$$F_I = \sqrt{\frac{2}{\pi\xi}\tan\frac{\pi\xi}{2}}\frac{0.923 + 0.199\left[1 - \sin\left(\frac{\pi\xi}{2}\right)\right]^4}{\sqrt{\cos\left(\frac{\pi\xi}{2}\right)}} \tag{29}$$

$$F_{II} = (3\xi - 2\xi^2)\frac{1.122 - 0.561\xi + 0.085\xi^2 + 0.18\xi^3}{\sqrt{1-\xi}} \tag{30}$$

Now substituting equations (20)-(28) into Eq.(19), we have,

$$c_{ij} = \frac{\partial^2}{E'\partial P_i\partial P_j}\int_o^a \left[\frac{P_1}{bh}\sqrt{\pi\xi}F_1 + \frac{3P_2L_c}{bh^2}\sqrt{\pi\xi}F_I + \frac{6P_3}{bh^2}\sqrt{\pi\xi}F_I\right]^2 + \left[\frac{P_2}{bh}\sqrt{\pi\xi}F_{II}\right]^2 d\xi \tag{31}$$

c_{ij} is the additional flexibility that results from the existence of a crack.

One considers the additional local flexibility due to the existence of the crack by updating the global stiffness matrix of the uncracked rotating beam. The updated stiffness matrix is calculated by replacing the corresponding terms in the uncracked beam stiffness element where the crack is introduced. The stiffness of the cracked element is obtained by adding the local flexibility cij due to the crack with the flexibility of the intact beam element. This is then used to find the local stiffness of the cracked element and substituted into the original stiffness matrix.

$$\sum_{e=1}^{N}(d_e^{sv})^T\{m_e^{sv}\ddot{d}_e^{sv} + 2\Omega g_e^{sv}\dot{d}_e^{sv} + [kc_e^{sv} + \Omega^2(s_e^{sv} - m_e^{sv}) + \dot{\Omega}g_e^{sv}]d_e^{sv}\} = \sum_{e=1}^{N}(d_e^{sv})^T f_e^{sv} \tag{32}$$

$$\sum_{e=1}^{N}(d_e^{w})^T[m_e^{w}\ddot{d}_e^{w} + (kc_e^{w} + \Omega^2 s_e^{w})d_e^{w}] = \sum_{e=1}^{N}(d_e^{w})^T f_e^{w} \tag{33}$$

where kc represent the stiffness of cracked beam.

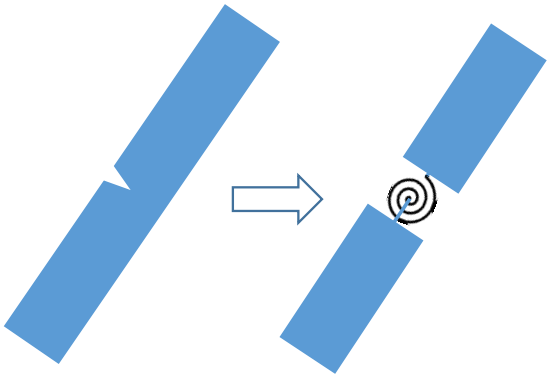

Figure 4. Modelling the crack as a massless torsional spring

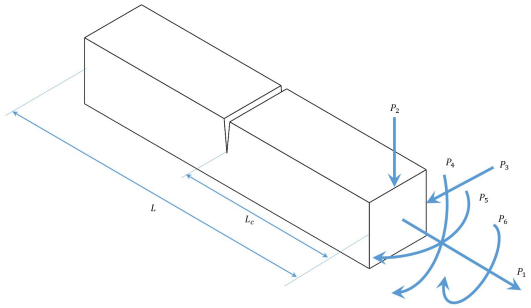

Figure 5. Beam with an open crack under generalized loading condition

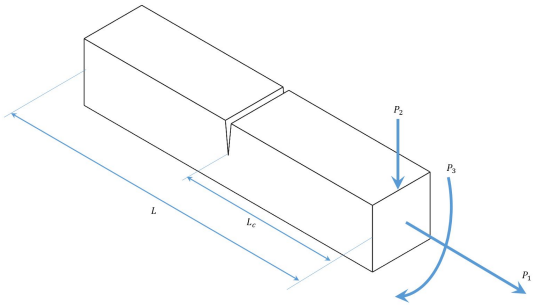

Figure 6. Beam with an open crack in-plane loads condition

3. Numerical results

For the convenience of discussion and for the sake of comparison with results in the literature, the following dimensionless parameters will be introduced.

$$\delta = \frac{r}{L}, \qquad \alpha = \sqrt{\frac{AL^2}{I_z}}, \qquad \gamma = \frac{\Omega}{\omega_{n_1}}, \qquad \varpi = \frac{\omega}{\omega_{n_1}}, \tag{34}$$

where δ, α, γ, ϖ and ω_{n_1} represent the hub ratio, the slenderness ratio, the angular speed ratio, the frequency ratio and fundamental natural frequency of non rotational cantilever beam.

3.1. Beam Without crack

The numerical simulation for the rotating intact cantilever beam are examined first. The results for the approaches (FE and the Rayleigh Ritz) for the dimensionless natural frequencies are compared in table 1. The mode shapes are also compared using the MAC as illustrated in Figures 7 and 8. The frequencies obtained are in good agreement with the previously published results [6].

In the MAC plot, in figure 7, the abscissa axis represents the mode shapes calculated by the Rayleigh-Ritz Method, and the ordinate axis represents the mode shapes calculated by the FEM. The red squares show the matching modes. When the cantilever beam is non-rotating, the MAC for the chordwise vibration is shown in figure 8. The 4th and 8th modes represent the longitudinal vibration likewise when the $\gamma = 7.11$ the 4th and 7th similar effect can be observed at $\gamma = 14.22$ and $\gamma = 28.44$.

Regarding the rotating speed, as in flapwise vibration, the natural frequencies are changing with the variation of the rotating velocity. Seemingly in figure 11, the existence of the gyroscopic coupling influences the bending and stretching modes created by a rotating movement, that results in the veering phenomena in the frequency versus speed plot. For example, when approximately the non-dimensional speed is $\gamma = 7.39$ the 3rd and 4th natural frequencies veer together whilst the 5th and 6th natural frequencies veer at about $\gamma = 17.06$. Likewise, veering occurs between the frequencies of the 6th & 7th modes, 7th & 8th modes for $\gamma = 10.52$ and $\gamma = 4.27$, respectively.

Figure 10 shows in detail the veering points for the lower dimensionless natural frequencies. The circles V1, V2 and V3 indicate the speed where pairs of natural frequencies exhibit the veering phenomena. The 3rd, 5th and 6th dimensionless natural frequencies correspond to the modes that are veering from being primarily bending vibration to longitudinal vibration at points V1 and V3. However, the 4th and the 6th are veering from predominating longitudinal vibration behaviour to bending vibration at points V1 and V2.

	frequency $\bar{\omega}$			
γ	**Chung and Yoo 2002**	**ANSYS**	**RRM**	**Error %**
0.000	1.002	1.003	1.002	0.006
0.284	1.049	1.050	1.049	0.000
0.569	1.179	1.179	1.179	0.000
0.853	1.367	1.367	1.367	0.002
1.138	1.591	1.591	1.591	0.000
1.422	1.838	1.836	1.838	0.000
1.706	2.097	2.095	2.097	0.001
1.991	2.365	2.362	2.365	0.000
2.275	2.638	2.634	2.638	0.000
2.560	2.914	2.909	2.914	0.001
2.844	3.192	3.186	3.192	0.000

Table 1. Comparison between different methods for flapwise dimensionless natural frequency calculated for a rotating cantilever beam

In general, increasing the rotating speed leads to an increase in the natural frequencies as shown in previous figures. There are additional factors that affect the natural frequencies of a rotating beam, which are not related to a crack such as hub ratio and slenderness as can be seen in figure 9 and figure 10, respectively. An increase in the hub ratio leads to an increase in the natural frequencies as shown in figure 9, due to a proportional relationship between the stiffness and the centrifugal force.

An increase in the slenderness leads to a decreased chance of veering at low frequencies, since the beam becomes thinner and more capable of bending rather than stretch. Decreasing slenderness ratio means a thicker cross section and the higher probability of veering at low frequencies.

Another noticeable fact is the existence of instability when the fundamental natural frequency of the chordwise vibration reduces to zero. This speed can be defined as the buckling speed, e.g. see [22] and [6].

3.2. Beam with a crack

A finite element model of a cracked beam can, consequently, be simulated using the formulation in equations (32) and (33). The crack model utilizes a cantilever beam with a crack on a single

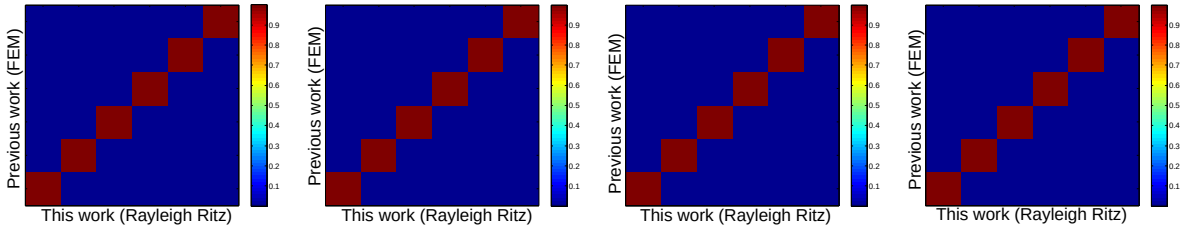

(a) MAC in flapwise vibration at γ=0 (b) MAC in flapwise vibration at γ=7.11 (c) MAC in flapwise vibration at γ=14.22 (d) MAC in flapwise vibration at γ=28.44

Figure 7. MAC for the flapwise vibration

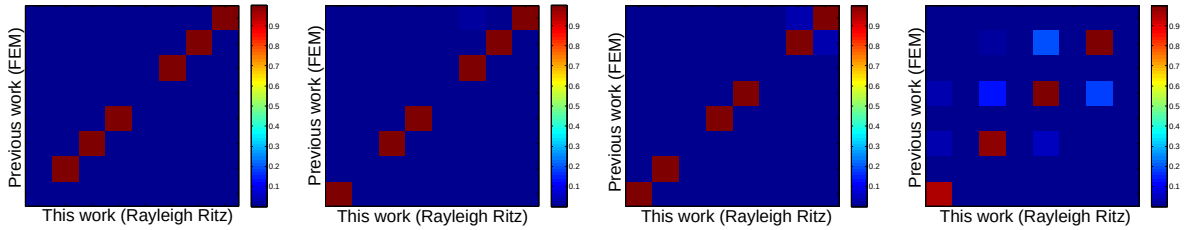

(a) MAC for the chordwise vibration at γ=0 (b) MAC in chordwise vibration at γ=7.11 (c) MAC in chordwise vibration at γ=14.22 (d) MAC in chordwise vibration at γ=28.44

Figure 8. MAC in chordwise vibration

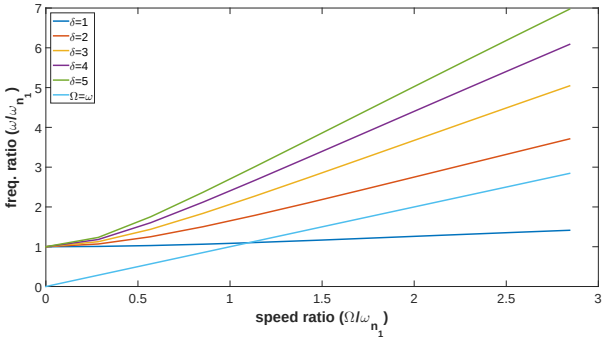

Figure 9. The effect of the hub ratio (δ) on the fundamental dimensionless natural frequency (ϖ) for different dimensionless rotating speed (γ)

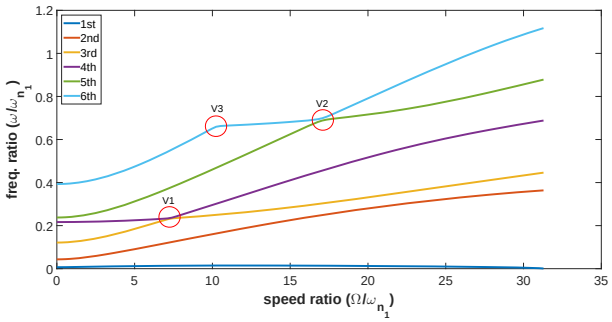

Figure 10. Dimensionless natural frequencies (ϖ) versus dimensionless rotation speed (γ). The red circles indicate the veering of modes.

edge, in order to compare the results with a solid finite element model assembled in a commercial FE code ANSYS, as presented in figure 13. In figure 14 the numerical simulations are shown for the beam with a crack at its midpoint for two different crack depths. The two results are in excellent agreement. There are numerous factors that affect the natural frequencies related to cracks, for example, the depth of the crack, its location and the orientation of the crack according to the direction of the loads [20].

Figure 14, shows that when the depth is equal to half the beam thickness i.e. $a = h/2$, the dimensionless natural frequencies for a crack at the root of the beam drops to 0.78, while for a crack depth less than $a = h/3$ the frequency ratio is about 0.91. A deeper crack leads to a

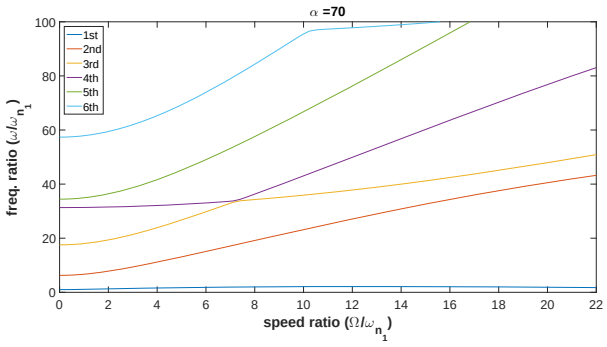

Figure 11. Chordwise vibration natural frequencies of a rotating cantilever beam at $\alpha = 70$

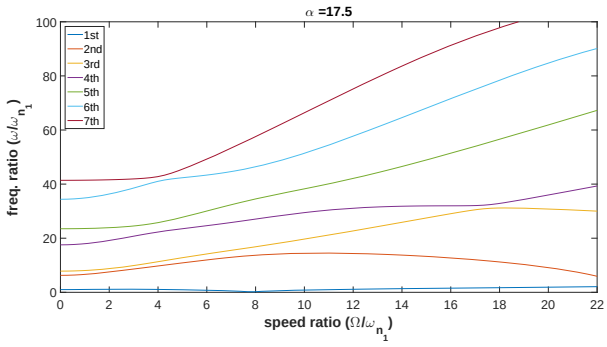

Figure 12. Chordwise vibration natural frequencies of a rotating cantilever beam at $\alpha = 17.5$

greater reduction in the frequency than a shallow one because of the additional flexibility, as expected.

Examining the crack location, it appears that when the crack is close to the root of the beam, i.e. close to the end which is attached to the hub, the effect of the crack becomes more significant and conversely this effect reduces when the crack is closer to the free end. This results from the bending moment effect at the fixed end. In addition, the crack effect vanishes or is negligible at some frequencies when it is located at a node of the higher order modes. This becomes evident in the results for the second and higher modes. Table 2 shows the agreement between the present work and an ANSYS FE model using solid elements. The maximum percentage error is 0.33% for the fundamental natural frequency at $\gamma = 0$ and 0.66% in the second natural frequency for the non-rotating beam.

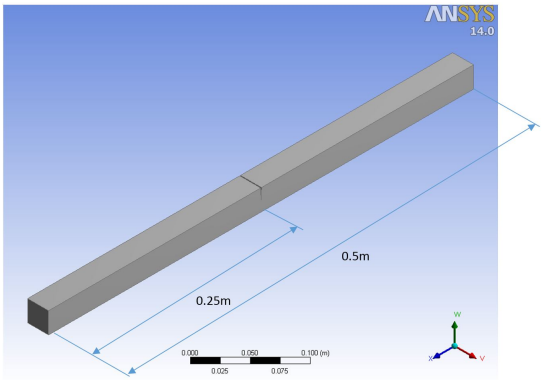

Figure 13. cracked beam

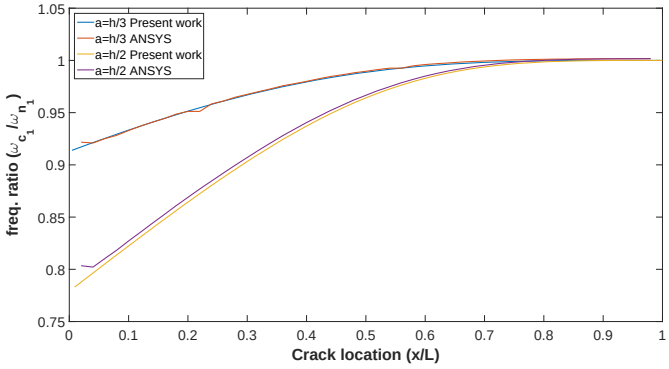

Figure 14. Comparison between the present work and an ANSYS FE model for the relative fundamental frequency of the cracked stationary cantilever beam

Considering the influence of the two main parameters, the crack location and the rotating speed, in one graph is figure 15, one can observe a clear picture of how the crack reduces the natural frequency. In addition, it can give a pre-estimation of the possible crack location.To assist the identification of the crack location the results are shown using the same two parameters in a 3D plot of the second relative natural frequency as shown in figure 16.

Utilizing the fundamental natural frequency chart in figure 15 side by side with the second

	1st ϖ			2nd ϖ		
γ	**present work**	**ANSYS**	**Error %**	**present work**	**ANSYS**	**Error %**
0.000	0.966	0.969	0.335	5.476	5.512	0.661
0.284	1.016	1.019	0.269	5.526	5.561	0.629
0.569	1.153	1.154	0.136	5.675	5.706	0.542
0.853	1.348	1.350	0.160	5.914	5.937	0.395
1.138	1.579	1.580	0.049	6.232	6.249	0.257
1.422	1.830	1.829	0.023	6.619	6.626	0.113
1.706	2.092	2.091	0.070	7.061	7.060	0.026
1.991	2.362	2.359	0.105	7.549	7.538	0.150
2.275	2.636	2.632	0.134	8.073	8.052	0.262
2.560	2.913	2.908	0.163	8.626	8.595	0.360
2.844	3.191	3.185	0.189	9.202	9.161	0.445

Table 2. Comparison between the present work and an ANSYS FE model for a single edge cracked rotating beam

natural frequency in figure 16, a better estimation of a crack location can be provided when the crack occurs in the second half of the beam, where the fundamental frequency has a low sensitivity to the crack location. Figure 17 and 18 clearly show the sensitivity of the two lowest natural frequencies of a rotating beam with respect to the crack location for a fixed rotating speed.

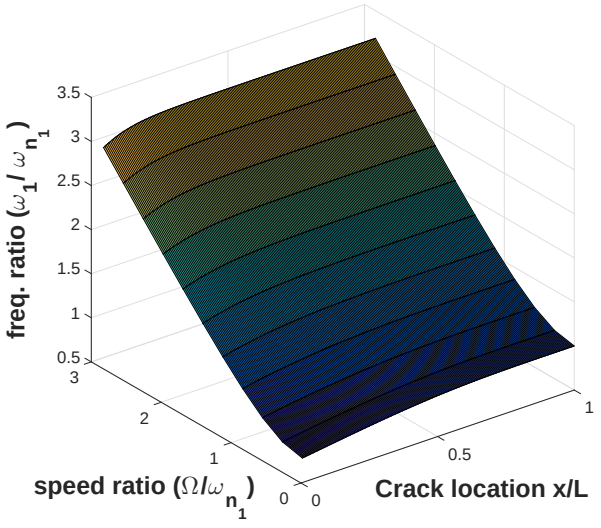

Figure 15. The first relative natural frequency for variable crack location and rotating speed. Crack depth $a = h/2$

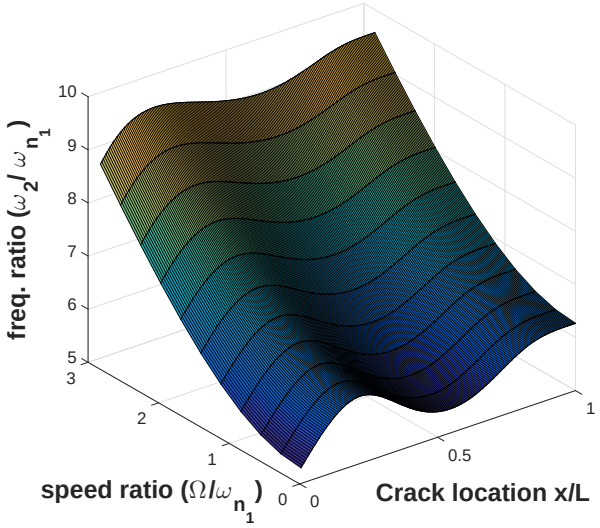

Figure 16. The second relative natural frequency for variable crack location and rotating speed. Crack depth $a = h/2$

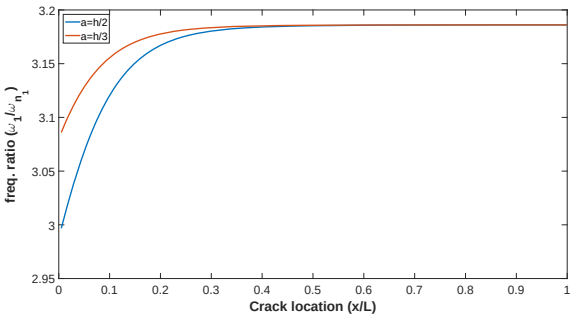

Figure 17. The effect of the crack's depth and location on the 1st relative natural frequency. Relative speed $\gamma = 2.844$

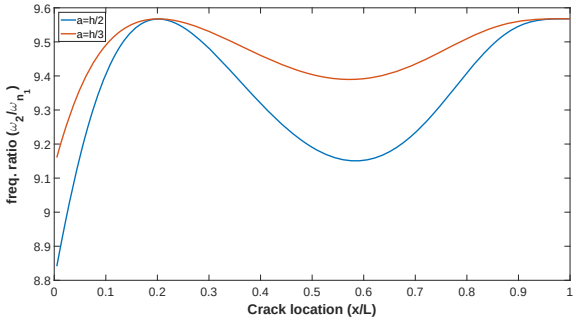

Figure 18. The effect of crack's depth and location on the 2nd relative natural frequency. Relative speed $\gamma = 2.844$

4. Conclusions

This study intended to model and investigate the dynamics of rotating beams with a crack, considering the effect of the rotational speed on the dynamic characteristics for such beams. Two approaches were used in modelling the rotating beam, both are based on Euler-Bernoulli beam theory. Firstly, a continuous system approach for flapwise vibration is developed. This method based on force equilibrium led to the derivation of the equation of motion. Rotational effects are included by simply adding a centrifugal force to the differential equation. Secondly, an energy method using Hamilton's principle provided the derivation of the equations of motion from the kinetic energy, potential energy and work done on the system, for the flapwise and chordwise equations of motion. Furthermore, a crack was introduced and modelled as a massless spring by using fracture mechanics and the Paris equation.

An outcome of the energy method is that it shows the coupling effect between the stretch and chordwise motion, while the flapwise equation is not coupled. Relating to the crack problem, it is divided into two models according to the direction of motion i.e. flapwise or chordwise. For the flapwise situation it needs two degrees of freedom for each element node (lateral direction and slope), whilst in the chordwise direction it needs three degrees of freedom for each node (lateral direction, longitudinal direction and slope) because of the combined bending and stretch motion.

Two different numerical methods were used to solve the equations of motion; the Rayleigh-Ritz method for the intact rotating beam where the finite element method are used for both the intact and cracked rotating beams.

The numerical results were presented and discussed in detail for rotating beams with and without cracks. For the flapwise motion, the natural frequencies monotonically increase with increasing rotational speed. No critical angular speed, i.e. where the critical speed means any natural frequency equals the rotational speed, arises . The increase in the hub ratio also increases these natural frequencies. Various parameters were considered and their effects investigated with changes in the rotational speed, hub ratio, slenderness ratio, critical rotating speed, and inspection of the veering phenomena and buckling speed were explored. In addition, the effect of the crack location and crack depth are explored and illustrated in three dimensional charts for the cracked rotating beam.

Regarding chordwise motion, the natural frequencies do not increase monotonically due to the gyroscopic coupling. A critical angular speed can occur though. There is the existence of a buckling speed, i.e. where the buckling speed causes the beam natural frequency to reduce to zero as the rotational speed increases. Slenderness and hub ratio have a significant effect on the critical angular speed, since the thinner beams tends to bend more than stretch.

For the cracked beams flapwise motion, the crack location has a significant effect on the natural frequencies. The closer the crack is to the hub, the lower are the natural frequencies. Generally there is an inverse relationship between the crack depth and the natural frequency. When a crack is located at one of the nodes of vibration of a particular mode then the frequency of that mode is unaffected.

Acknowledgements
The lead author gratefully acknowledges the Ministry of Higher Education and Scientific Research in Iraq for providing full PhD scholarship.

References

[1] Rubinstein N and Stadter J T 1972 *Journal of the Franklin Institute* **294** 217–229 ISSN 00160032
[2] Bhat R 1986 *Journal of Sound and Vibration* **105** 199–210
[3] Yoo H and Shin S 1998 *Journal of Sound and Vibration* **212** 807–828 ISSN 0022460X
[4] Rao S and Gupta R 2001 *Journal of Sound and Vibration* **242** 103–124 ISSN 0022460X
[5] Cai G P, Hong J Z and Yang S X 2004 *International Journal of Mechanical Sciences* **46** 871–889 ISSN 00207403
[6] Chung J and Yoo H 2002 *Journal of Sound and Vibration* **249** 147–164 ISSN 0022460X
[7] Yang J, Jiang L and Chen D 2004 *Journal of Sound and Vibration* **274** 863–875 ISSN 0022460X
[8] Banerjee J, Su H and Jackson D 2006 *Journal of Sound and Vibration* **298** 1034–1054 ISSN 0022460X
[9] Yoo H H, Cho J E and Chung J 2006 *Journal of Sound and Vibration* **290** 223–241 ISSN 0022460X
[10] Özdemir Ö and Kaya M 2006 *Journal of Sound and Vibration* **289** 413–420 ISSN 0022460X
[11] Kim H, Hee Yoo H and Chung J 2013 *Journal of Sound and Vibration* **332** 5917–5928 ISSN 0022460X
[12] Banerjee A and Pohit G 2014 *Procedia Technology* **14** 188–195 ISSN 22120173
[13] Cheng Y, Yu Z, Wu X and Yuan Y 2011 *Finite Elements in Analysis and Design* **47** 825–834 ISSN 0168874X
[14] Qian G L, Gu S N and Jiang J S 1990 *Journal of Sound and Vibration* **138** 233–243 ISSN 0022460X
[15] Behera K and K V 2014 *Procedia Engineering* **86** 835–842 ISSN 1877-7058
[16] Yoo H, Ryan R and Scott R 1995 *Journal of Sound and Vibration* **181** 261–278 ISSN 0022460X
[17] Silani M, Ziaei-Rad S and Talebi H 2013 *Applied Mathematical Modelling* **37** 9907–9921 ISSN 0307904X
[18] Zheng D and Kessissoglou N 2004 *Journal of Sound and Vibration* **273** 457–475 ISSN 0022460X
[19] Tada H, Paris P C and Irwin G R 2000 *The Stress Analysis of Cracks Handbook* (ASME Press) ISBN 9780791801536
[20] Ibrahim A M, Ozturk H and Sabuncu M 2013 *Structural Engineering and Mechanics* **45** 33–52
[21] Ozturk H, Yashar A and Sabuncu M 2016 *Mechanics of Advanced Materials and Structures* **23** 715–726
[22] Lima M A C F 2012 *Rotating Cantilever Beams : Finite Element Modeling and Vibration Analysis* Ph.D. thesis Faculdade de Engenharia da Universidade do Porto